Journal of the Mechanics and Physics of Solids 138 (2020) 103920

Contents lists available at ScienceDirect

Journal of the Mechanics and Physics of Solids

journal homepage: www.elsevier.com/locate/jmps

Characterizing poroelasticity of biological tissues by spherical indentation: An improved theory for large relaxation

Ming Wang[a,b,c,1], Shaobao Liu[c,d,1], Zhimin Xu[e], Kai Qu[b,f], Moxiao Li[b,e], Xin Chen[b,e], Qing Xue[b,e], Guy M. Genin[a,b,g], Tian Jian Lu[c,d,*], Feng Xu[a,b,*]

[a] The Key Laboratory of Biomedical Information Engineering of Ministry of Education, School of Life Science and Technology, Xi'an Jiaotong University, Shaanxi 710049, PR China
[b] Bioinspired Engineering & Biomechanics Center (BEBC), Xi'an Jiaotong University, Xi'an 710049, PR China
[c] State Key Laboratory of Mechanics and Control of Mechanical Structures, Nanjing University of Aeronautics and Astronautics, Nanjing 210016, PR China
[d] Nanjing Center for Multifunctional Lightweight Materials and Structures, Nanjing University of Aeronautics and Astronautics, Nanjing 21006, PR China
[e] State Key Laboratory for Strength and Vibration of Mechanical Structures, School of Aerospace, Xi'an Jiaotong University, Xi'an 710049, PR China
[f] Department of Hepatobiliary Surgery, The First Affiliated Hospital of Xi'an Jiaotong University, Xi'an 710061, PR China
[g] National Science Foundation Science and Technology Center for Engineering Mechanobiology, Washington University, St. Louis 63130, MO, United States

ARTICLE INFO

Article history:
Received 22 May 2019
Revised 6 January 2020
Accepted 18 February 2020
Available online 3 March 2020

Keywords:
Mechanical characterization
Porous biomaterials
Shear modulus, Poisson ratio
Diffusion coefficient

ABSTRACT

Flow of fluids within biological tissues often meets with resistance that causes a rate- and size-dependent material behavior known as poroelasticity. Characterizing poroelasticity can provide insight into a broad range of physiological functions, and is done qualitatively in the clinic by palpation. Indentation has been widely used for characterizing poroelasticity of soft materials, where quantitative interpretation of indentation requires a model of the underlying physics, and such existing models are well established for cases of small strain and modest force relaxation. We showed here that existing models are inadequate for large relaxation, where the force on the indenter at a prescribed depth at long-time scale drops to below half of the initially peak force (i.e., $F(0)/F(\infty) > 2$). We developed an indentation theory for such cases of large relaxation, based on Biot theory and a generalized Hertz contact model. We demonstrated that our proposed theory is suitable for biological tissues (e.g., porcine liver, spleen, kidney, skin and human cirrhosis liver) with both small and large relaxations. The proposed method would be a powerful tool to characterize poroelastic properties of biological materials for various applications such as pathological study and disease diagnosis.

* Corresponding authors.
E-mail addresses: tjlu@nuaa.edu.cn (T.J. Lu), fengxu@mail.xjtu.edu.cn (F. Xu).
[1] The authors contributed equally to this paper.

https://doi.org/10.1016/j.jmps.2020.103920
0022-5096/

1. Introduction

Many biological tissues show time-dependent, poroelastic properties arising from resistance to the fluid flow by a porous scaffold, which play important roles in their physiological functions (Cowin, 1999; Mow and Hayes, 1991; Mow et al., 1984; Simon, 1992; Han et al., 2020). Analogous to the Biot theory of soil compaction, the poroelastic properties of biological tissues arise from a combination of the mechanical properties of the scaffold and the transport properties of the fluid within the scaffold (Biot, 1941). The most typical example of poroelastic tissue is cartilage, where the scaffold is predominantly collagen and charged proteoglycans, and the fluid phase is predominantly water (Mow et al., 1984), which plays an important role in energy dissipation and nutriment transport (Mow et al., 1980a; Nia et al., 2011). Many other tissues (e.g., liver, cornea, arterial endothelium and the intervertebral disc) exhibit poroelasticity as well (Eisenberg and Grodzinsky, 1987; Kenyon, 1979; Malandrino et al., 2015; Ricken et al., 2010; Hu et al., 2017). Disruption of poroelastic properties is a hallmark of a range of pathologies. For instance, liver fibrosis results in the change of poroelastic properties of liver tissue, where upregulation of perisinusoidal collagen (in the space of Disse) stiffens matrix and decreases blood perfusion and tissue permeability (Wells, 2013; Bataller and Brenner, 2005). Similar changes to poroelasticity also occur in renal (Youhua, 2006) and pulmonary fibrosis (Knudsen et al., 2017), attenuating bio-mass transfer and exacerbating pathology. Therefore, understanding the poroelastic properties (i.e., interplay between scaffold mechanics and fluid permeability) of biological tissues is of great importance for the diagnosis and treatment of these pathologies (Butcher et al., 2009; Frantz et al., 2010; Levental et al., 2009).

Palpation is the clinical standard for qualitative mechanical characterization of biological tissues (Ezzat et al., 1994). Inferring quantitative mechanical properties and permeability from palpation requires performing a calibrated indentation through fitting a theoretical poroelastic model with a displacement-controlled load relaxation test or force-controlled creep test (Hu et al., 2010; Lin et al., 2007; Mow et al., 1980a). The first theoretical poroelastic solution designed for interpretation of indentation experiments was derived for the biphasic theory by Mak et al. (1987), who obtained the solution for stress-relaxation and creep behavior of articular cartilage. More recently, Oyen and co-workers developed a set of a computational algorithm and master curves for interpretation of experiments involving a sphere indenter indented a gel with a linear force ramp (Oyen, 2011, 2013). To further simplify the approach, Hu et al. (2011a, 2010) and Hui et al. (2010) and Lin and Hu, 2006 obtained semi-analytical solutions by finite element method between the initial pressed load and completely relaxed (infinite time) load of rigid indenters in different shapes (i.e., flat circular, rectangular, conical and spherical). The analysis has been successfully used to obtain poroelastic properties of various soft materials including biological tissues (Hu et al., 2011; Mauck et al., 2003; Moeendarbary et al., 2013; Oyen, 2015). However, the theoretical models used in fitting are typically derived by neglecting the liquid transport as induced by deformation over the timescale of the indentation, which may be not applicable when force relaxation is substantial. For example, recent studies have reported negative Poisson ratios in hydrogels (Strange et al., 2013; Wang et al., 2014) and liver tissues (Ahn and Kim, 2010) when force relaxes to below half of the peak indentation force. These measurements are unreasonable because uniaxial tests reveal positive Poisson ratios for both liver (0.04–0.33 (Chen et al., 2011)) and PVA gels (0.34–0.5 (Urayama et al., 1993)).

To meet this need for a more accurate theory of poroelastic indentation, it is more reasonable by considering the fluid-flow-induced deformation during the indentation process. We modeled fluid flow during both the indentation and isometric holding in an indentation test by combining Biot theory with Hertz contact theory. Using this improved model, we characterized several poroelastic properties of biological tissues, including shear modulus, Poisson ratio and diffusion coefficient. Our theory approached prior small-relaxation theory asymptotically for small relaxation, showing prospects for characterizing a broad range of biological materials and tissues and also for detecting changes to poroelasticity associated with diseases.

2. Materials and methods

2.1. Large relaxation indentation theory

We developed an indentation theory that included fluid flow during both the indentation and the isometric holding of an indentation test by combining Biot theory with Hertz contact theory. Following the work of Biot and other soft hydrated tissue models (Biot, 1941; Mow et al., 1980b), we treated the indented tissue as linear, isotropic, and poroelastic, and fully saturated with solvent throughout the indentation process. We considered the axisymmetric, small strain, large displacement problem of indentation in a semi-infinite space (Fig. 1B).

2.1.1. Governing equations

2.1.1.1. Kinematics. The linearized, axisymmetric, strain fields within the tissue at each time t can be written in terms of a radial displacement field, $u(r, z, t)$, and a vertical displacement field, $w(r, z, t)$, in a cylindrical (r, θ, z) coordinate system:

$$\varepsilon_r(r,z,t)=\frac{\partial u(r,z,t)}{\partial r},\ \varepsilon_\theta(r,z,t)=\frac{u(r,z,t)}{r},\ \ \varepsilon_z(r,z,t)=\frac{\partial w(r,z,t)}{\partial z},\ \varepsilon_{zr}(r,z,t)=\frac{1}{2}\left(\frac{\partial u(r,z,t)}{\partial z}+\frac{\partial w(r,z,t)}{\partial r}\right) \tag{1}$$

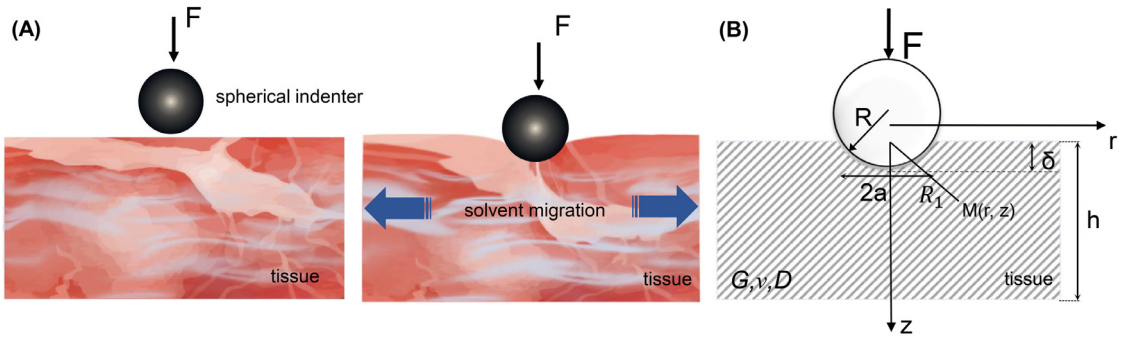

Fig. 1. *Indentation schematic diagram.* (A) Indentation test of poroelastic properties of biological tissues. (B) Axisymmetric problem of indentation in a semi-infinite space and cylindrical coordinates. The parameters G, ν and D are the Poisson ratio, shear modulus and diffusion coefficient of the biological tissue, respectively; a is the contact radius between the indenter and the tissue.

where ϵ_r, ϵ_θ, and ϵ_z are the diagonal terms of the strain tensor ϵ; ϵ_{zr} is the only non-zero shear term. For a tissue fully saturated with solvent, the volumetric dilatation (volume change per unit volume) $e = \text{trace}(\epsilon)$ represents the change in solvent volume per unit tissue volume. In the following, unless otherwise noted, all variables are functions of r, z, and t.

2.1.1.2. Constitutive equations. A linear poroelastic material consists of a linearly elastic, porous scaffold, permeated by a fluid phase (Rudnicki, 2001). Most homogenizations of these phases, including the MAK biphasic model of cartilage (Mow et al., 1980b), arise from a treatment analogous to that of Biot theory (Biot, 1941). For isotopically poroelastic materials, the constitutive model is (Rudnicki, 2001):

$$\boldsymbol{\sigma} = 2G\epsilon + \left(\frac{2G\nu}{1-2\nu}e - p\right)\boldsymbol{I} \tag{2}$$

where $\boldsymbol{\sigma}$ is the linearized stress tensor; $\boldsymbol{I}$ is the identity tensor; G and ν are the shear modulus and Poisson ratio of the scaffold in the absence of fluid, respectively; p is the pore fluid pressure. This constitutive law is purely elastic, but is made to vary with time by considering a pressure-gradient driven volumetric rate of flow, $\boldsymbol{q}$. According to Darcy's law:

$$\boldsymbol{q} = -K\nabla p \tag{3}$$

where K is constant of proportionality in Darcy's law between the fluid flux vector (volumetric fluid discharge per unit time and per unit area) and the pressure gradient. K, which is often referred to as the hydraulic permeability (Childs, 1952), has units of $m^2/(Pa\ s)$ and is the ratio of the intrinsic permeability of the tissue and the dynamic viscosity of the solvent.

2.1.1.3. Equilibrium equations. For cases such as indentation in which body forces are negligible compared to other forces, and for cases in which inertial terms are small, the stress fields satisfy the equilibrium conditions:

$$\begin{aligned}\frac{\partial\sigma_r}{\partial r} + \frac{\partial\tau_{zr}}{\partial z} + \frac{\sigma_r - \sigma_\theta}{r} = 0\\ \frac{\partial\tau_{zr}}{\partial r} + \frac{\partial\sigma_z}{\partial z} + \frac{\tau_{zr}}{r} = 0\end{aligned} \tag{4}$$

2.1.1.4. Boundary and initial conditions. Analogous to the Boussinesq solution for an elastic half-space subjected to a vertical concentrated force (Green and Zerna, 1992), traction free boundary conditions were applied to the surface of the tissue outside of the indenter, and stresses approached zero infinitely far from it. For intermediate tissue in a region beneath the indenter, with a radius ρ greater the contact radius of indenter, the applied force F is balanced by the normal stress at each depth z:

$$F + \int_0^\rho 2\pi r\sigma_z dr = 0 \tag{5}$$

The initial displacement fields are $u = w = 0$ at time $t = 0$.

2.1.2. Solution

Based on the Boussinesq solution and Hertz contact theory, we deduced the relationship between the time-dependent applied force and the indentation depth by considering poroelasticity during both loading and holding. Substituting Eqs. (1), (2) into Eq. (4), we rewrote the equilibrium equations as:

$$\frac{1}{1-2\nu}\frac{\partial e}{\partial r} + \nabla^2 u - \frac{u}{r^2} - \frac{1}{G}\frac{\partial p}{\partial r} = 0 \tag{6}$$

$$\frac{1}{1-2\nu}\frac{\partial e}{\partial z}+\nabla^2 w-\frac{1}{G}\frac{\partial p}{\partial z}=0 \tag{7}$$

where the axisymmetric Laplace operator is $\nabla^2=\frac{\partial^2}{\partial r^2}+\frac{1}{r}\frac{\partial}{\partial r}+\frac{\partial^2}{\partial z^2}$. The problem was solved by separation of variables, with $p=f_1(t)f_2(r,z)$, so that the general solution of Eqs. (6),(7) is given by:

$$\begin{aligned} u(r,z,t)&=U_1 f_1(t)+U_0(r,z)\\ w(r,z,t)&=W_1 f_1(t)+W_0(r,z)\end{aligned} \tag{8}$$

Eq. (8) reveals that the total displacement can be decomposed into the displacements due to fluid transport and the elastic deformation of solid.

The mass conservation of pore fluid can be stated as the continuity equation div $\boldsymbol{q}=-\partial e/\partial t$ (Biot, 1941), namely:

$$\frac{\partial q_r}{\partial r}+\frac{q_r}{r}+\frac{\partial q_z}{\partial z}=-\frac{\partial}{\partial t}\left(\frac{\partial u}{\partial r}+\frac{u}{r}+\frac{\partial w}{\partial z}\right) \tag{9}$$

Due to the independence of the variables, we obtain:

$$q_r=-\frac{\partial u}{\partial t}\ ,\ \ q_z=-\frac{\partial w}{\partial t} \tag{10}$$

Substituting Eq. (10) into Eq. (3) and observing the separated variable form of p, we obtain:

$$\frac{\partial u}{\partial t}=-K\frac{\partial f_2(r,z)}{\partial r}f_1(t),\ \ \frac{\partial w}{\partial t}=-K\frac{\partial f_2(r,z)}{\partial z}f_1(t) \tag{11}$$

so that the general solution of Eq. (8) is:

$$u=-K\frac{\partial f_2(r,z)}{\partial r}\int f_1(t)dt,\ \ w=-K\frac{\partial f_2(r,z)}{\partial z}\int f_1(t)dt \tag{12}$$

Comparing Eq. (8) and Eq. (12) reveals that $f_1(t)$ should have an exponential form:

$$f_1(t)=\exp\left(-t/\tau_p\right) \tag{13}$$

where τ_p is the poroelastic relaxation time-scale, which can be written:

$$\tau_p=\frac{a^2}{D} \tag{14}$$

in which a is the radius of the spherical contact and D is the diffusion coefficient (Chan et al., 2012; Lin and Hu, 2006). Here, the diffusion coefficient represents the constant of proportionality, in the absence of pressure gradients, of the gradient of the solvent volume fraction within the porous tissue matrix and the flux of solvent per unit time and per unit area through that matrix (Detournay and Cheng, 1993). Based on the Boussinesq solution, U_0 and W_0 (displacement duo to elastic deformation) in Eq. (8) are given by (Sneddon, 1965):

$$\begin{aligned} U_0&=C_1\frac{rz}{R_1^3}+C_2\frac{r}{R_1(R_1+z)}\\ W_0&=C_1\left[\frac{z^2}{R_1^3}+(3-4\nu)\frac{1}{R_1}\right]+\frac{C_2}{R_1}\end{aligned} \tag{15}$$

where C_1 and C_2 are constants, $R_1=\sqrt{r^2+z^2}$. Combining Eq. (15) with the initial conditions and the boundary conditions in Eq. (5), the displacement equation is given by:

$$\begin{aligned} u&=\frac{F}{4\pi G}\left[\frac{rz}{R_1^3}-(1-2\nu)\frac{r}{R_1(R_1+z)}\right](1-\exp\left(-t/\tau_p\right))\\ w&=\frac{F}{4\pi G}\left[\frac{2(1-\nu)}{R_1}-\frac{z^2}{R_1^3}\right](1-\exp\left(-t/\tau_p\right))\end{aligned} \tag{16}$$

We assume that the spherical indenter is rigid, and that the substrate is elastic and semi-infinite. According to the Hertz solution (Hertz, 1896, 1882) for contact between elastic bodies and combining with Eq. (16), we obtain the relationship between the time-dependent applied force F and the indentation depth δ:

$$F(t)=F_{Hertz}(\delta,R)\frac{1}{1-\exp\left(-t/\tau_p\right)} \tag{17}$$

where $F_{Hertz}(\delta,R)=\frac{8}{3}\delta^{\frac{3}{2}}R^{\frac{1}{2}}\frac{G}{1-\nu}$, the $F_{Hertz}(\delta,R)$ is initial force of the elastic basement from the Hertz solution, G is the shear modulus of the scaffold, and ν is Poisson ratio, and R is the radius of the spherical indenter. This satisfies the initial condition that $u=F=0$ at $t=0$. Setting t_0 as the time needed for the indenter to be pushed from $u(t=-t_0)=0$ to $u(t=0)=\delta_{max}$,

in which δ_{max} is the maximum displacement, at which the indenter is held, and applying the time coordinate transform, Eq. (17) can be rewritten as:

$$F(t) = \begin{cases} F_{Hertz}(u(t), R)\left(\dfrac{1}{1 - Aexp\left(-\frac{t}{\tau_p}\right)}\right), -t_0 \le t \le 0 \\ F_{Hertz}(\delta_{max}, R)\left(\dfrac{1}{1 - Aexp\left(-\frac{t}{\tau_p}\right)}\right), t > 0 \end{cases} \tag{18}$$

where $A \approx \exp(-t_0/\tau_p)$ is a coefficient that quantifies the effect of solvent diffusion during indentation ($-t_0 \le t \le 0$) on subsequent force relaxation ($t > 0$), and F_{Hertz} is the force for a displacement δ_{max} predicted for linear elasticity by the Hertz contact model. The coefficient A thus represents a correction factor that accounts for fluid flow during indentation. For fast loading, in which the loading timescale t_0 is much smaller than the poroelastic timescale τ_p (that is, the Deborah number t_0/τ_p is very small), A approaches unity. However, the poroelastic material properties (i.e., shear modulus, Poisson ratio and diffusion coefficient) are not affected by the loading speed.

2.2. Sample preparation

Fresh samples of porcine liver, kidney, spleen and skin were obtained from a local abattoir in Xi'an, Shaanxi, China. An apple of the species *Malus pumila* was obtained from a local farm. All specimens were preserved at 4 °C and tested within a few hours of acquisition. Cirrhotic human liver tissues were obtained a local hospital, and the experiments were performed within 24 h of resection (**Fig. S3**). This study was approved by ethic committee of the first affiliated hospital of Xi'an Jiaotong university. Porcine organs, apple, and human tissues were cut into 3 cm × 3 cm rectangular specimens that were 2.5 cm thick. Glisson's capsule was removed from the liver. All tissues were allowed to swell to equilibrium in 4 °C saline for 3 h. Porcine skin tissue was cut to 3 cm × 3 cm rectangular specimens that were 0.5 mm thick and allowed to swell to equilibrium in 4 °C colza oil for 5 h.

2.3. Indentation testing

Indentation by metal spheres of four different diameters ($2R$ = 10 mm, 5 mm, 4 mm and 3 mm) was used to characterize the biological tissues poroelastic properties. The indenter consisted of a stainless steel ball bonded to a hollow stainless steel tube (**Fig. S1**). Following standard protocols to ensure that the substratum did not affect the indentation (Hu et al., 2011a; Hu et al., 2010;), we ensured in all cases that the sample thickness h was large enough compared to the radius $a = \sqrt{R\delta}$ of the indenter contact area, in which δ is the depth of indentation:

$$h > 8\sqrt{R\delta} \tag{19}$$

For the spherical indenters of diameter 10 mm, 5 mm, 4 mm and 3 mm, we set δ to 3 mm, 2.5 mm, 2 mm and 1.5 mm, respectively. For porcine skin tissue, we applied δ = 1 mm due to its limited thickness.

Experiments were performed on a Bose ElectroForce 3220 (Bose Corporation, Framingham, MA) using a load sensor with a force resolution of 0.001 N and a displacement resolution of 0.01 μm (**Fig. S1**). Before performing displacement control tests, the indenter tip was adjusted to a position slightly above the surface, and proceeded with indentation to a fixed depth δ at a speed of 0.5 mm/s. The indenter was held isometrically for a time interval sufficient to enable relaxation. This time interval was based upon the characteristic poroelastic relaxation time τ_p. This time interval is size-dependent, and scales as $\tau_p \approx a^2/D = R\delta/D$, in which D is the diffusion coefficient of the solvent in the tissue. We chosed the data collection time during relaxation based upon the maximum value of $R\delta$ and upon results of initial tests. For liver, spleen, and apple, $R\delta$=30 mm^2, and $\tau_p^{liver} \approx \tau_p^{spleen} \approx \tau_p^{apple} \approx 100$ s. For kidney, diffusion was slower and $\tau_p^{kidney} \approx 440$ s. $R\delta$ was substantially smaller for skin, so that $\tau_p^{skin} \approx 500$ s. To ensure adequate data for curve-fitting, the indenter was thus held at the fixed depth δ for 350 s of relaxation for liver and spleen specimens, and for 900 s for the other tissues; this time was substantially longer than needed for the apple tissue. For load control tests, the indenter touched with a preload of approximately 1 μN.

In each of the displacement-controlled relaxation tests, the solvent in the tissues migrated, affecting the force on the indenter both in the rising period during indentation and the relaxation period during the isometric hold (Fig. 1& 5A). We repeated indentation tests at least three times at different locations for each of the four spherical indenters and their associated indentation depths.

2.4. Protocol for extracting poroelastic properties from indentation tests

Through fitting the indentation relaxation curve with the theoretical model, we characterized the poroelastic properties of several biological tissues, specifically the shear modulus, Poisson ratio, and diffusion coefficient. The protocol began with estimating the parameters A and τ_p by fitting Eq. (18) to an experimentally measured stress relaxation curve using ordinary least squares (**Fig. S2**). The diffusion coefficient D could then be estimated from τ_p using Eq. (14). Following this, the Poisson

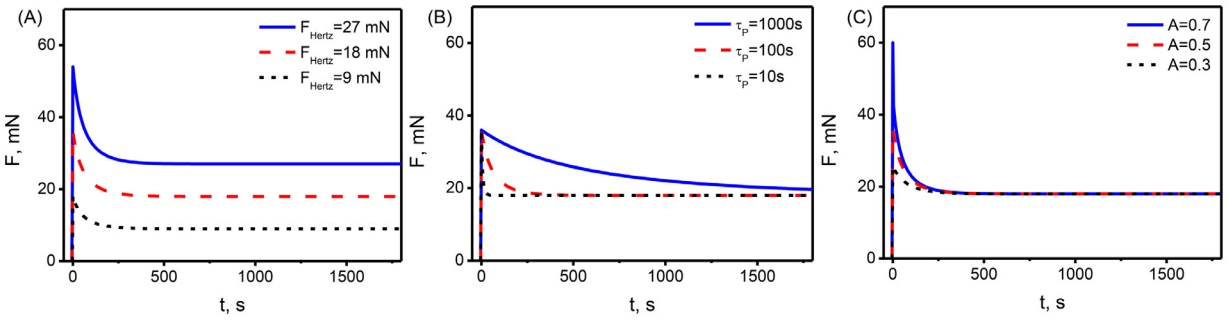

Fig. 2. *The force-relaxation curves for indentation of a poroelastic solid.* (A) The force required to indent a poroelastic material increases with indentation depth, but decreases as the indenter is held isometrically. The plateau is affected by the elastic properties of the material, represented by $F_{Hertz}(\delta_{max}, R)$. For all curves, the poroelastic time-scale is $\tau_p = 100$ s, and the fluid flow correction factor is $A = 0.5$. (B) The relaxation rate but not the peak or plateau was affected by τ_p. Here, $F_{Hertz}(\delta_{max}, R) = 18$ mN, and $A = 0.5$. (C) The peak force but not the plateau force or relaxation rate were affected by A. Here, $F_{Hertz}(\delta_{max}, R) = 18$ mN and $\tau_p = 100$ s.

ratio ν and shear modulus G were estimated by comparing the short-time and long-time response. At short times, the poroelasticity of tissue cannot be reflected, hence $\nu \approx 0.5$ is adopted when $t = 0$. However, due to the influence of pressing process on poroelastic relaxation curve, the relaxation force when $t = 0$ is distinguished from traditional indentation theory as shown in Eq. (20) (noted $1 - A$ is applied to modify F(0) in Eq. (21)):

$$F(0) = \frac{16}{3}\delta_{max}^{\frac{3}{2}} R^{\frac{1}{2}}\ G \tag{20}$$

$$F(0) = \frac{16}{3}\delta_{max}^{\frac{3}{2}} R^{\frac{1}{2}} \frac{G}{1-A} \tag{21}$$

At long time-scales, after the fluid within the specimen equilibrates with external fluid, the tissue behaves like a compressible elastic solid and:

$$F(\infty) = \frac{8}{3}\delta_{max}^{\frac{3}{2}} R^{\frac{1}{2}} \frac{G}{1-\nu} \tag{22}$$

The two limits are related as:

$$\frac{F(0)}{F(\infty)} = \frac{2(1-\nu)}{1-A} \tag{23}$$

where $F(0)/F(\infty)$ is the ratio between the peak force and steady force on the indenter (Fig. 5A). For biological tissues, the synergy between the relaxation amount $F(0)/F(\infty)$ and the correction factor A ensures that the Poisson ratio stays positive when approriate.

3. Results and discussion

3.1. The model fits poroelastic indentation force-displacement curves

The force required to indent a poroelastic material increases with indentation depth, but decreases with solvent flow away from the compressed region. Thereafter, as the indenter is held isometrically, the force needed to hold the indenter at a fixed depth relaxes over time with continued solvent flow (Fig. 1), which can be well predicted by our model (Fig. 2). The three parameters governing the response (i.e., force *v.s.* time) are the steady applied force, $F_{Hertz}(\delta_{max}, R)$, which comes from the Hertz solution, and two free fitting parameters, i.e., the poroelastic time-scale, τ_p, and the fluid flow correction factor, A. To assess the effect of these three parameters, we performed parameter analysis by changing values of each parameter (*e.g.* $F_{Hertz}(\delta_{max}, R)$, τ_p and A) in turn and controlling two parameters invariant (Fig. 2). We observed that $F_{Hertz}(\delta_{max}, R)$, associated with the elastic properties of the material, influences the peak value of the force-time curve, but not the rate of relaxation or the amplitude (Fig. 2A). Increasing the poroelastic relaxation time-scale, τ_p, slows the asymptotic approach to steady state (Fig. 2B). The correction factor $A \approx \exp(-t_0/\tau_p)$ quantifies the effect of solvent diffusion during indentation. This factor affects both the peak force and the relaxation rate as shown in Fig. 2C. The peak force scales as $1/(1-A)$, and therefore increases with increasing A. The degree of relaxation, $F(\infty)/F(0) = (1-A)$, also increases with increasing A. The poroelastic relaxation timescale τ_p is independent of A; however, for a given indentation ramp time t_0, A will increase with decreasing τ_p because more liquid will flow away during the indentation process.

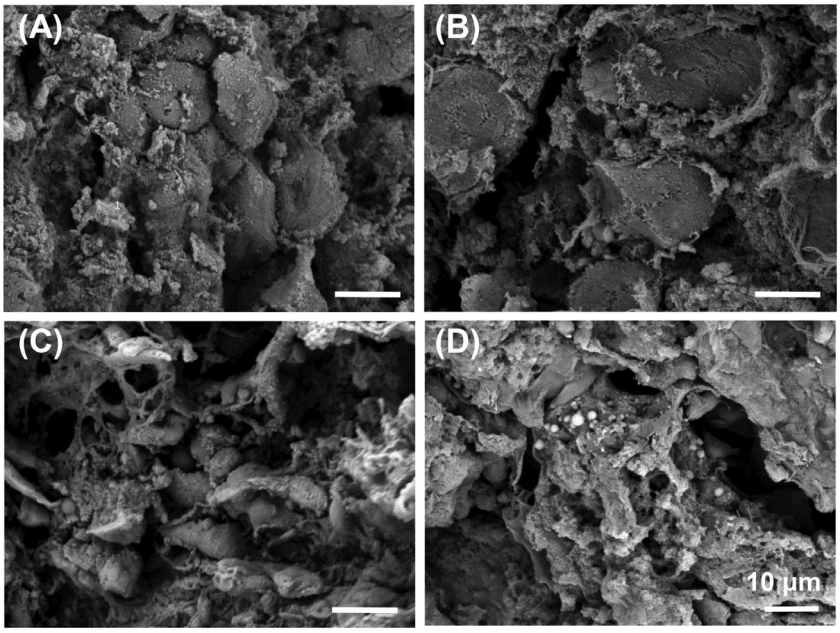

Fig. 3. *SEM images of biological tissues (porcine liver, cirrhotic human liver, porcine spleen and porcine kidney) show obvious porosity of the microstructure of different biological tissues.* (A) Dehydrated, fractured liver specimens showed the polyhedral, multifaceted hepatocytes which form one-cell-thick muralia separated by sinusoids. (B) Cirrhotic human liver showed fibrosis between hepatocytes. (C) Porcine spleen and (D) Porcine kidney showed similar porosity. Scale bars: 10 μm. (HITACHI TM-1000 scanning electron microscope).

3.2. Poroelastic properties could be extracted from indentation tests

Both viscoelasticity and poroelasticity contribute to force relaxation in most biological tissues, and distinguishing the contributions of these two factors is important. In biological tissues, viscoelasticity typically arises from conformational changes and breakage of transient bonds amongst macromolecules, processes for which the viscoelastic relaxation timescale (τ_v) is independent of lengthscales (Strange et al., 2013). Poroelasticity arises from resistance to fluid flow by a tissue's porous protein scaffold, so that the poroelastic relaxation timescale ($\tau_p = a^2/D$) increases with increasing lengthscale (Hu and Suo, 2012; Wang et al., 2014). To first order, viscoelastic timescales are material properties (Bird et al., 1987; Rowe et al., 2019), as is the diffusion constant for specific combinations of solvent and protein structure at a defined temperature, over a broad range of concentrations (Elson and Magde, 1974; Koppel et al., 1976; Magde et al., 1974). Both viscoelastic and poroelastic responses can be observed and quantified from the results of indentation tests.

As an example, we considered the case of a biomaterial whose viscoelastic and poroelastic properties are unknown. The material was indented by indenters of four different sizes that were pressed to fixed depth and held isometrically. The relaxation of force during this sustained isometric loading was recorded. The key to dissecting the poroelastic and viscoelastic responses is the normalization of these force versus time data (Fig. 4).

The un-normalized force versus time curves show the same general trends, with a peak force following indentation decaying to an asymptote over time intervals of 10–350 s (Fig. 4A). The peak force and long-relaxation asymptotes increase with increasing indenter size.

Insight into the underlying physical processes can be found be renormalizing the force and time to account for potential underlying physics. The first model to check is elasticity. Consistent with linear elasticity and the Hertz solution, the peak indentation force in Fig. 4A increased with indentation depth, but the force decay evident in that figure rules out an elastic response for the material. The next model to check is linear viscoelasticity. At the initial peak and at the asymptote, force, displacement, and indenter size should be related by the Hertz solution. When the isometric force is renormalized by $3a\delta/4$, the Hertz solution predicts that the quantity $3F(0)a\delta/4$ should be a constant that, for a relatively rigid indenter, equals $E(0)/(1-\nu(0)^2)$; for infinite time in a linear viscoelastic material, the asymptote should be $3F(\infty)a\delta/4 = E(\infty)/(1-\nu(\infty)^2)$. However, neither the peaks nor the asymptotes in Fig. 4B meet at a single point, indicating that linear viscoelasticity is not the correct model for the material.

The next model to evaluate is poroelasticity. For this, the renormalization arises from the diffusion timescale, which scales as $\tau_p \sim a^2/D$. According to Eq. (18), renormalizing the time as t/a^2 should thus make the curves collapse to a single master curve. The curves do indeed collapse onto a master curve for $t/a^2 > 10$ s/m^2 but diverge over shorter times (Fig. 4C). This indicates that the tissues are poroelastic at long times, but exhibit both poroelastic and viscoelastic behavior at shorter times. Therefore, we can decouple the viscoelastic effect through fitting the long-term poroelastic relaxation.

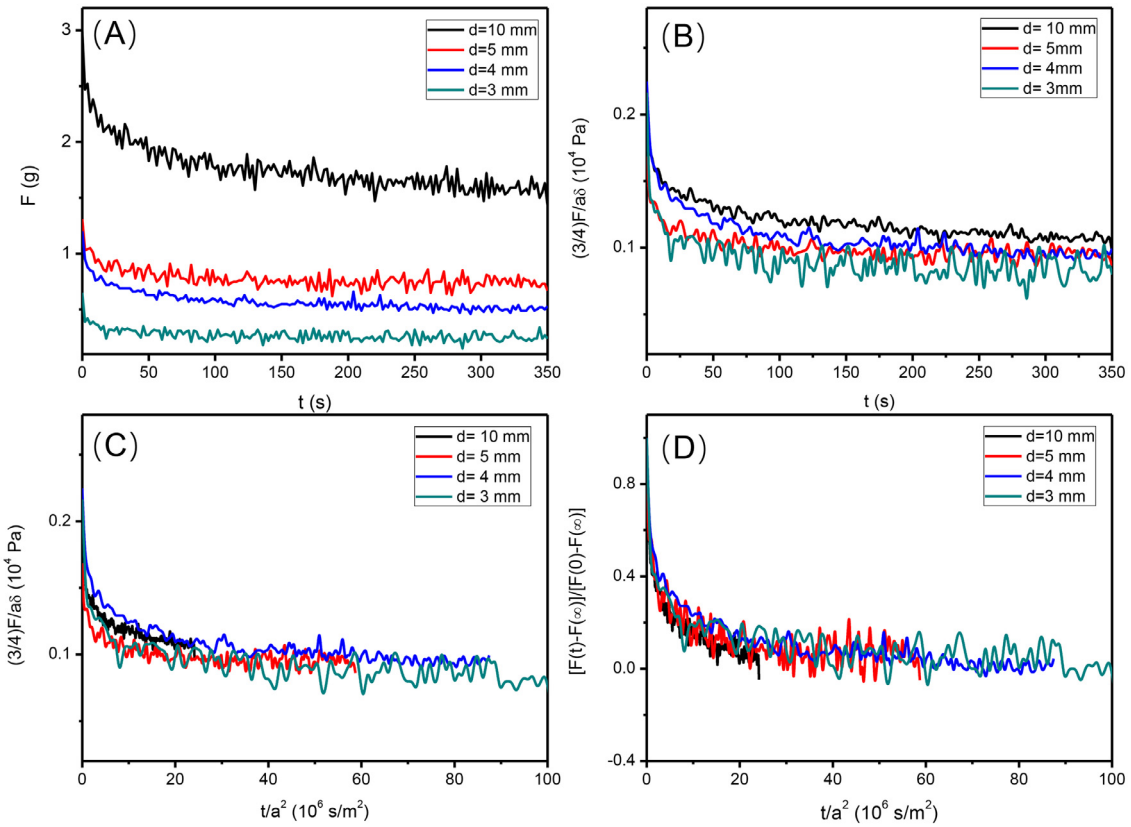

Fig. 4. *Analysis of isometric force versus time curves during indentation of liver tissue with indenters of four different diameters.* (A) Following a ramped indentation (data not shown), the peak force for indentation increased with increasing indenter size. The isometric force subsequently relaxed over time. These results showed that the material is not elastic. (B) The first normalization used is that appropriate for linear viscoelasticity, in which the isometric force curves should converge into one curve when normalized as $F/a\delta$. However, a clear size dependence was evident, indicating that the material was either nonlinear viscoelastic or poroelastic. (C) When time is additionally renormalized as appropriate for poroelasticity, the curves collapse onto a master curve for longer timscales, indicating a transition from some combination of viscoelasticity and poroelasticity to pure poroelasticity. (D) Normalized relaxation function $[F(t) - F(\infty)]/[F(0) - F(\infty)]$, assuming that the end point of each experiment represents a fully relaxed state, versus renormalized time t/a^2.

Another way to view this is in the context of a normalized relaxation function, $g(\tau) = [F(t) - F(\infty)]/[F(0) - F(\infty)]$ (Fig. 4D). When plotted against renormalized time t/a^2, and when approximating the experimental endpoint as the fully relaxed state of the material, the curves further collapse into a single master curve, once more suggesting that poroelastic effects contribute throughout the relaxation process.

For the liver tissue studied in Fig. 4, the viscoelastic time scale is ~10 s and the poroelastic time scale is ~100 s. This separation of scales is evident in a number of other tissues as well in millimeter scale experiments. In kidney the dominant viscoelastic time scale of 50 s (Mattice et al., 2011) is much faster than the poroelastic timescale of 440 s; in hydrogels the dominant viscoelastic time scale of 100 s (Wang et al., 2014) is much faster than the poroelastic time scale of 10^5 s; in PDMS, the dominant viscoelastic timescale of 10 s (Hu et al., 2011a) is much faster than the poroelastic time scale of 10^4 s. Although most viscoelastic materials exhibit a spectrum of such responses (Babaei et al., 2016b; Xu et al., 2013) especially when nonlinearity is considered (Babaei et al., 2017; Fung, 2013; Provenzano et al., 2002), the separation of scales for the dominant time constants enables a poroelastic interpretation of data at slower timescales in these materials. Furthermore, remodeling of tissue by cells can alter these viscoelastic response spectra, the timescales for this are typically slow compared to the poroelastic responses (Babaei et al., 2016a); remodeling of cells themselves can occur, especially in response to mechanical force, but these occur over time intervals of 10 of seconds (Krishnan et al., 2009; Lee et al., 2012; Nekouzadeh et al., 2008). Taken together, these factors enable the application of the present model to the poroelastic characterization of a range of biological tissues.

Through fitting our model to indentation relaxation curves, we characterized the poroelastic properties of several biological tissues and quantified their shear modulus, Poisson ratio, and diffusion coefficient. The protocol for interpreting experimental relaxation curves began with choosing A and τ_p in Eq. (18) to fit the data using ordinary least squares (**Fig. S2**). If the peak and steady state values of the force are known with sufficient reliability, this can be achieved directly from Eqs. (22) and (23).

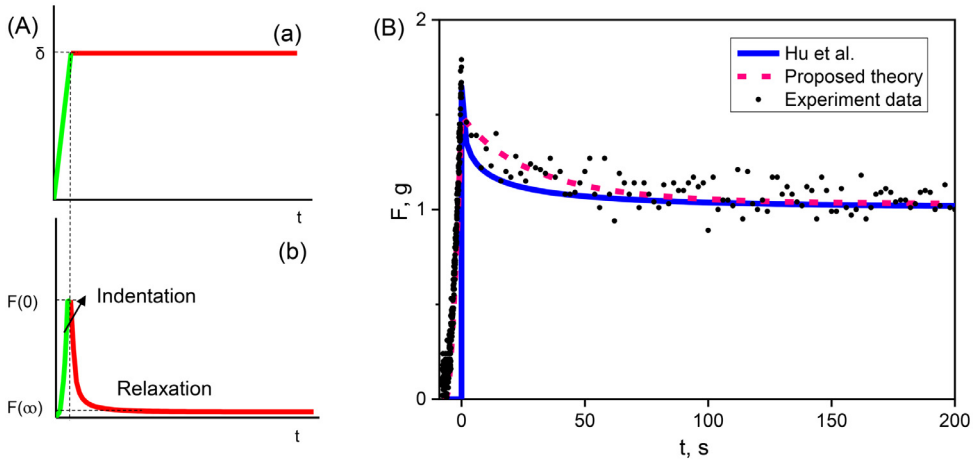

Fig. 5. *Displacement and force curves, and comparison of methods.* (A) Force response of a poroelastic tissue to a ramp-and-hold indentation test. The green line represents the indentation process and the red line represents the relaxation process. (B) The loading curve and subsequent relaxation are better fit by the proposed method than by the method of Hu et al. (Hu et al., 2010).

The first tissue studied was porcine liver tissue in normal saline. Based on Eq. (23), the Poisson ratio was obtained as $\nu = 0.39 \pm 0.026$, which is on the order of published values for porcine liver ($\nu = 0.04 - 0.33$) from uniaxial stretching (Chen et al., 2011). Based on Eq. (22) and the steady state force $F(\infty)$, the shear modulus was estimated as $G = 0.31 \pm 0.070$ kPa, which falls into the range of previously reported rheological test results ($G = 0.3 - 1$ kPa). (Marchesseau et al., 2010; Wells, 2013).

Because the time scale $\tau_p = a^2/D = R\delta_{max}/D$ is related to the diffusion coefficient D (Detournay and Cheng, 1993), D could be estimated from the data as well. The diffusion coefficient was obtained, $D = (1.6 \pm 0.91) \times 10^{-7}$ m^2/s, which is within the reported range for various mammalian liver tissues (Stock et al., 2010). We also observed that the estimates of Poisson ratio, shear modulus, and diffusion coefficient were relatively insensitive to the size of spherical indenters, the indentation depth (**Table S1**), and the loading speed (**Table S2**).

3.3. The indentation and isometric portions of the force relaxation curve

We compared our predictions to those of the model of Hu et al., in two ways, again using the data for porcine liver (Fig. 5B). Our predictions account for fluid flow during both the indentation and isometric relaxation, and, as expected, provide a vastly superior fit of the indentation force versus time curve. Our predictions have a better fit for the overall force versus time trend in the relaxation portion. The model of Hu et al., has a superior fit of the initial force peak, but then predicts that relaxation occurs quickly. Our model misses the initial peak, suggesting that multiple timescales of poroelasticity and/or viscoelasticity are at work in the porcine liver specimen. As mentioned above, both viscoelasticity and poroelasticity contribute to force relaxation in most biological tissues, with the viscoelastic relaxation timescale (τ_v) independent of lengthscales (Strange et al., 2013) and the poroelastic relaxation timescale ($\tau_p = a^2/D$) increasing with increasing lengthscale (Hu and Suo, 2012; Wang et al., 2014). At the millimeter scale, the poroelastic timescale (~100 s) is longer than viscoelastic time scale (~10 s) for liver tissue. Thus, relaxation in liver under our testing conditions is viscoelasticity-dominated over the short term and poroelasticity-dominated over the long term. Therefore, we could decouple the viscoelastic effect by fitting only the long-term poroelastic relaxation, with the correction factor A reflecting the effect of solvent diffusion only. In addition, because the poroelastic relaxation model is a linear model, multiple poroelastic timescales can be added through superposition, in much the same way that Maxwell elements are combined in the Generalized Maxwell model (Bird et al., 1987).

Next, we compared predictions of normalized force ($g(\tau) = \frac{F(t)-F(\infty)}{F(0)-F(\infty)}$) versus the normalized time ($\tau = Dt/a^2$) for a material with small relaxation (e.g., PDMS) (**Fig. S4**). We observed that both models are able to predict the relaxation with the normalized force asymptoting to zero over time, demonstrating that our proposed theory is applicable for the full range of small-to-large relaxation.

3.4. Validation against and application to a broad range of biological tissues

To extend the applicability of the proposed theory for biological tissues, we characterized several poroelastic properties of biological tissues (e.g., spleen, kidney, skin and human cirrhosis liver), including shear modulus, Poisson ratio and diffusion coefficient (Fig. 6 and **Table S3**). From the perspective of experimental analysis, the fundamental shortcoming of the model

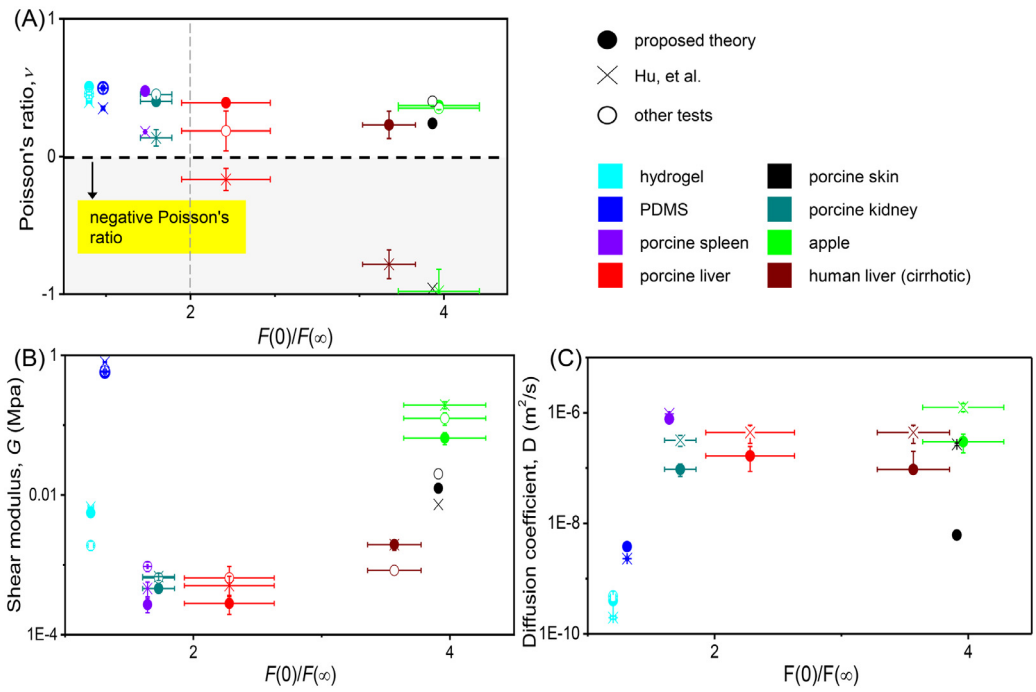

Fig. 6. *The proposed poroelastic indentation theory improves upon prior models by correctly predicting positive Poisson ratios.* (A) Poisson ratio ν, (B) shear modulus G and (C) Diffusion coefficient D predicted for indentation tests using the proposed theory and the model of Hu et al (Hu et al., 2010). Data shown are from the following sources: (Poisson ratio ν: liver (Chen et al., 2011), kidney (Hostettler et al., 2010), apple (Dintwa et al., 2008), skin (Choi and Zheng, 2005), hydrogel (Takigawa et al., 1996), PDMS (Müller et al., 2019); shear modulus, G: hydrogel (Chippada et al., 2010), PDMS (Xiang et al., 2013), liver (Marchesseau et al., 2010), kidney (Umale et al., 2013), spleen (Nicolle et al., 2012), skin (Kirkpatrick et al., 2004), apple (Dintwa et al., 2008), human liver (Palmeri et al., 2008); diffusion constant: hydrogel (Ju et al., 2010)). The indentation curves of hydrogel and PDMS used in the proposed theory was captured in Kalcioglu et al., 2012 and Hu et al., 2011a.

of Hu et al., is that it predicts negative Poisson ratios for tissues that undergo large relaxation (Fig. 6A). These include the porcine liver described above, and cirrhotic human liver ($F(0)/F(\infty) \sim 3.6$), porcine kidney ($F(0)/F(\infty) > \sim 1.7$), porcine spleen ($F(0)/F(\infty) > \sim 1.6$), and porcine skin ($F(0)/F(\infty) > \sim 3.9$).

Our method outperforms that of Hu et al., in that it predicts positive Poisson ratios that are consistent with results obtained from tensile and compressive tests in literature (Fig. 6A). We observe that the deviation from experimental data of predictions using the method of Hu et al., increases with the degree of relaxation, $F(0)/F(\infty)$. Predictions of Poisson ratio using that method become negative for large relaxation, $F(0)/F(\infty) > 2$, despite experimental data from other methods to the contrary. Predictions obtained using our method are consistent with those obtained using other methods for tissues with both large and small relaxations.

The diffusivity D and shear modulus G estimated from experimental data using our proposed theory are relaxation-independent. These estimates agree with those obtained using the method of Hu et al., and are likewise on the order of other experimental results (Fig. 6B&C). For instance, for porcine kidney, our estimate of $G = 0.46 \pm 0.052$ kPa is on the order of that using the method of Hu et al. ($G = 0.68 \pm 0.080$ kPa), and neither estimate has a statistically significant difference from previously published ($G = 0.32 \pm 0.41$ kPa) (Umale et al., 2013). By combining the Biot theory for poroelastic media with the Darcy's law and the continuity equation, the relationship between the diffusion coefficient and the hydraulic permeability can be written as (Hu et al., 2010): $D = (2G\,(1-\nu))/((1-2\nu))\,K$, where G and ν are the shear modulus and Poisson ratio of the drained network respectively, K is the hydraulic permeability, and D is the diffusion coefficient. According to this relationship, the hydraulic permeability of biological tissues can be obtained from diffusion coefficient. Our estimates of transport properties result in slightly lower hydraulic permeabilities than other results, as is expected due to the accounting for fluid flow during indentation: models that do not account for this must force predictions of fluid flow "catch up" to with the fluid flow that is ignored during indentation, and must do so by predicting a greater hydraulic permeability. The hydraulic permeability of porcine liver tissue estimated using the proposed theory is 1.8 m^2/GPa s, whereas those reported by others range from 8.6–110 m^2/GPa s (Kerdok, 2006). The hydraulic permeability of a hydrogel estimated using the proposed theory is 1.2 $\times 10^{-4}$ m^2/GPa s, whereas that reported using a transport through membrane test is 1.3 $\times 10^{-4}$ m^2/GPa s (Yasuda et al., 1971). Our results show that, using the proposed method, we can characterize a broad range of biological tissues and biomaterials with shear modulus ranging from ~0.1 kPa for brain (Bayly et al., 2012) to ~GPa of bone (Hinz, 2000; Osterhoff et al., 2016).

To demonstrate potential diagnostic value for the proposed method, we performed an indentation test and cirrhotic human liver tissues (**Fig. S3**). Cirrhosis, a stage in the progression of liver fibrosis, is characterized by extracellular matrix protein (e.g., collagen) accumulation in Disse gap's (Fig. 3B), which stiffens the tissue (Schuppan and Afdhal, 2008; Wells, 2013). Cirrhosis further attenuates transport in liver tissue as resistance and pressure in portal tracts increases, along with that in associated collateral circulation through shunts (Malay and Rameshbabu, 2012). Our estimate for the Poisson ratio of that tissue is $\nu = 0.23 \pm 0.099$, which is significantly different from the values associated with healthy liver tissues of $\nu = 0.4 - 0.5$ (Hostettler et al., 2010), suggesting a possible metric for diagnosis. These indentations also show elevated shear modulus of $G = 0.83 \pm 0.032$ kPa, compared to that of healthy human liver tissue with a shear modulus of 0.3 kPa (Marchesseau et al., 2010). The theory of Hu et al., provides a higher estimate of shear modulus based upon our measurements, with $G = 1.9 \pm 0.32$ kPa. The diffusion coefficient we obtained is $D = 0.94 \times 10^{-7}$ m^2/s, on the same order of magnitude as the estimate using the theory of Hu et al., $D = 2.1 \times 10^{-7}$ m^2/s.

For materials with smaller relaxation, the predictions of both approaches are similar. For PDMS, we obtained $G = 5.54 \pm 0.183$ kPa and $D = 4.0 \times 10^{-10}$ m^2/s, while the method of Hu et al., gave $G = 6.70 \pm 0.050$ kPa and $D = 1.97 \times 10^{-10}$ m^2/s. The diffusion coefficient is comparable to the values reported in the literature (Ju et al., 2010).

4. Conclusions

By modifying a spherical indentation model to characterize the poroelastic properties of biological tissues, we were able to improve the estimation of poroelastic material properties in three ways. The first is the elimination of internal inconsistencies in the interpretive model that lead to predictions of negative Poisson ratios when these are not expected. We note that, despite this internal inconsistency, previous models are capable of fitting and replicating force relaxation data. This is a well-known problem in viscoelastic fitting, and has been explored extensively in the context of other models. A commonly cited example of this is Fung's quasilinear viscoelastic (QLV) theory, which can often replicate relaxation data without having the capacity to predict the response of the material under different loading conditions (Babaei et al., 2015; Lakes and Vanderby, 1999; Provenzano et al., 2001). However, these inadequacies of underlying viscoelastic models are well known to introduce substantial error into extrapolations of fittings to new loading scenarios (Babaei et al., 2018, 2017; Lakes and Vanderby, 1999; Provenzano et al., 2001). In the context of the current model, the prediction of negative Poisson ratios for many tissues will lead to such error.

Second, in addition to being free of unfortunate internal inconsistencies such as a negative Poisson ratio, our proposed theory can predict the entire indentation and isometric force relaxation experiment. This provides a vastly superior fit of the indentation force versus time curve, as was shown in Fig. 5B.

Finally, we also emphasize that, although prior theories can handle the limiting case of small scale relaxation (**Fig. S4**), it cannot handle large scale relaxation without incorrectly predicting a negative Poisson ration. The modifications in our proposed theory are required to accommodate large relaxation; we validated this for $1.6 < \frac{F(0)}{F(\infty)} < 3.9$.

Declaration of Competing Interest

The authors declare that they have no known competing financial interests or personal relationships that could have appeared to influence the work reported in this paper.

CRediT authorship contribution statement

Ming Wang: Methodology, Formal analysis, Writing - original draft. **Shaobao Liu:** Conceptualization, Methodology, Writing - original draft. **Zhimin Xu:** Methodology. **Kai Qu:** Resources. **Moxiao Li:** Visualization, Writing - review & editing. **Xin Chen:** Investigation. **Qing Xue:** Investigation. **Guy M. Genin:** Supervision, Writing - review & editing. **Tian Jian Lu:** Supervision, Writing - review & editing, Funding acquisition. **Feng Xu:** Supervision, Writing - review & editing, Funding acquisition.

Acknowledgement

This work was financially supported by the National Natural Science Foundation of China (11532009, 11972280, 11972185 and 11902155), by the Natural Science Foundation of Jiangsu Province (BK20190382), by the foundation of Jiangsu Provincial Key Laboratory of Bionic Functional Materials, by the Foundation for the Priority Academic Program Development of Jiangsu Higher Education Institutions, by the Open Fund of the State Key Laboratory of Mechanics and Control of Mechanical Structures (MCMS-I-0219K01 and MCMS-E-0219K02) of China, by the National Science Foundation through the Science and Technology Center for Engineering Mechanobiology (CMMI 1548571) and by the NIH through grant U01EB016422.

Supplementary materials

Supplementary material associated with this article can be found, in the online version, at doi:10.1016/j.jmps.2020.103920.

References

Ahn, B., Kim, J., 2010. Measurement and characterization of soft tissue behavior with surface deformation and force response under large deformations. Med. Image Anal. 14, 138–148.

Babaei, B., Abramowitch, S.D., Elson, E.L., Thomopoulos, S., Genin, G.M., 2015. A discrete spectral analysis for determining quasi-linear viscoelastic properties of biological materials. J. Royal Soc. Interface 12, 20150707.

Babaei, B., Davarian, A., Lee, S.-.L., Pryse, K.M., McConnaughey, W.B., Elson, E.L., Genin, G.M., 2016a. Remodeling by fibroblasts alters the rate-dependent mechanical properties of collagen. Acta Biomater. 37, 28–37.

Babaei, B., Davarian, A., Pryse, K.M., Elson, E.L., Genin, G.M., 2016b. Efficient and optimized identification of generalized maxwell viscoelastic relaxation spectra. J. Mech. Behav. Biomed. Mater. 55, 32–41.

Babaei, B., Velasquez-Mao, A., Pryse, K.M., McConnaughey, W.B., Elson, E.L., Genin, G.M., 2018. Energy dissipation in quasi-linear viscoelastic tissues, cells, and extracellular matrix. J. Mech. Behav. Biomed. Mater. 84, 198–207.

Babaei, B., Velasquez-Mao, A.J., Thomopoulos, S., Elson, E.L., Abramowitch, S.D., Genin, G.M., 2017. Discrete quasi-linear viscoelastic damping analysis of connective tissues, and the biomechanics of stretching. J. Mech. Behav. Biomed. Mater. 69, 193–202.

Bataller, R., Brenner, D.A., 2005. Liver fibrosis. J. Clin. Invest. 115, 209–218.

Bayly, P.V., Clayton, E.H., Genin, G.M., 2012. Quantitative imaging methods for the development and validation of brain biomechanics models. Ann. Rev. Biomed. Eng. 14, 369–396.

Biot, M.A., 1941. General theory of three-dimensional consolidation. J. Appl. Phys. 12, 155–164.

Bird, R.B., Armstrong, R.C., Hassager, O., 1987. Fluid Mechanics. Dynamics of polymeric liquids. Wiley, New York.

Butcher, D.T., Alliston, T., Weaver, V.M., 2009. A tense situation: forcing tumour progression. Nat. Rev. Cancer 9, 108–122.

Chan, E.P., Hu, Y., Johnson, P.M., Suo, Z., Stafford, C.M., 2012. Spherical indentation testing of poroelastic relaxations in thin hydrogel layers. Soft Matter 8, 1492–1498.

Chen, X., Nakayama, M., Tsujita, T., Jiang, X., 2011. Identification of physical properties of swine liver for surgical simulation using a dynamic deformation model. In: Proceedings of the IEEE/SICE International Symposium on System Integration, pp. 655–660.

Childs, E., 1952. The measurement of the hydraulic permeability of saturated soil in situ I. principles of a proposed method. Proc. Royal Soc. Lond. Ser. A. Math. Phys. Sci. 215, 525–535.

Chippada, U, Yurke, B, Langrana, N A, 2010. Simultaneous determination of Young's modulus, shear modulus, and Poisson's ratio of soft hydrogels. J. Mater. Res. 25, 545–555.

Choi, A.P., Zheng, Y.P., 2005. Estimation of young's modulus and poisson's ratio of soft tissue from indentation using two different-sized indentors: finite element analysis of the finite deformation effect. Med. Biol. Eng. Comput. 43, 258–264.

Cowin, S.C., 1999. Bone poroelasticity. J. Biomech. 32, 217–238.

Detournay, E., Cheng, A.H.-D., 1993. Fundamentals of poroelasticity. In: Hudson, J.A. (Ed.). Comprehensive Rock Engineering: Principles, Practices and Projects, vol. 2. Pergamon Press, Oxford, UK, pp. 113–171.

Dintwa, E., Zeebroeck, M.V., Ramon, H., Tijskens, E., 2008. Finite element analysis of the dynamic collision of apple fruit. Postharvest Biol. Technol. 49, 260–276.

Eisenberg, S. R., Grodzinsky, A. J., 1987. The kinetics of chemically induced nonequilibrium swelling of articular cartilage and corneal stroma. J. Biomech. Eng. 109, 79–89.

Elson, E.L., Magde, D., 1974. Fluorescence correlation spectroscopy. I. Conceptual basis and theory. Biopolym.: Orig. Res. Biomol. 13, 1–27.

Ezzat, S., Sarti, D.A., Cain, D.R., Braunstein, G.D., 1994. Thyroid incidentalomas. prevalence by palpation and ultrasonography. Arch. Intern. Med. 154, 1838–1840.

Frantz, C., Stewart, K.M., Weaver, V.M., 2010. The extracellular matrix at a glance. J. Cell. Sci. 123, 4195–4200.

Fung, Y. C., 2013. Biomechanics: mechanical properties of living tissues. Springer Science & Business Media.

Green, A.E., Zerna, W., 1992. Theoretical Elasticity. Courier Corporation.

Han, Y L, Pegoraro, A F, Li, H, et al., 2020. Cell swelling, softening and invasion in a three-dimensional breast cancer model Nat. Phys. 16, 101–108.

Hertz, H.R., 1882. Ueber Die Beruehrung Elastischer Koerper (On Contact Between Elastic Bodies), 1. Gesammelte Werke (Collected Works).

Miscellaneous Papers Hertz, H., 1896. Über die berührung fester elastischer körper (On the contact of rigid elastic solids). In: Jones, Schott (Eds.), J. Reine Und Angewandte Mathematik 92. Macmillan, London, p. 156 (1896).

Hinz, B., 2000. Matrix mechanics and regulation of the fibroblast phenotype. Periodontol 2000 63, 14–28.

Hostettler, A., George, D., Rémond, Y., Nicolau, S.A., Soler, L., Marescaux, J., 2010. Bulk modulus and volume variation measurement of the liver and kidneys in vivo using abdominal kinetics during free breathing. Comput. Methods Prog. Biomed. 99, 149–157.

Hu, Y., Chen, X., Whitesides, G., Vlassak, J., Suo, Z., 2011a. Indentation of polydimethylsiloxane submerged in organic solvents. J. Mater. Res. 26, 785–795.

Hu, J, Jafari, S, Han, Y, et al., 2017. Size-and speed-dependent mechanical behavior in living mammalian cytoplasm. Proc Natl Acad Sci U S A 114, 9529–9534.

Hu, Y., Suo, Z., 2012. Viscoelasticity and poroelasticity in elastomeric gels. Acta Mech. Solida Sin. 25, 441–458.

Hu, Y., You, J.-.O., Auguste, D.T., Suo, Z., Vlassak, J.J., 2011c. Indentation: a simple, nondestructive method for characterizing the mechanical and transport properties of pH-sensitive hydrogels. J. Mater. Res. 27, 152–160.

Hu, Y., Zhao, X., Vlassak, J.J., Suo, Z., 2010. Using indentation to characterize the poroelasticity of gels. Appl. Phys. Lett. 96, 121904.

Hui, C.Y., Yu, Y.L., Chuang, F.C., Shull, K.R., Lin, W.C., 2010. A contact mechanics method for characterizing the elastic properties and permeability of gels. J. Polym. Sci. Part B Polym. Phys. 44, 359–370.

Ju, H., Sagle, A.C., Freeman, B.D., Mardel, J.I., Hill, A.J., 2010. Characterization of sodium chloride and water transport in crosslinked poly(ethylene oxide) hydrogels. J. Memb. Sci. 358, 131–141.

Kalcioglu, Z.I., Mahmoodian, R., Hu, Y., Suo, Z., Van Vliet, K.J., 2012. From macro- to microscale poroelastic characterization of polymeric hydrogels via indentation. Soft Matter 8, 3393.

Kenyon, D. E., 1979. A mathematical model of water flux through aortic tissue. B. Math. Biol. 41, 79–90.

Kerdok, A., 2006. Characterizing the Nonlinear Mechanical Response of Liver to Surgical Manipulation. Havard University.

Kirkpatrick, S.J., Duncan, D.D., Fang, L., 2004. Low-frequency surface wave propagation and the viscoelastic behavior of porcine skin. J. Biomed. Opt. 5474, 1311–1319.

Knudsen, L., Ruppert, C., Ochs, M., 2017. Tissue remodelling in pulmonary fibrosis. Cell Tissue Res. 367, 607–626.

Koppel, D., Axelrod, D., Schlessinger, J., Elson, E., Webb, W., 1976. Dynamics of fluorescence marker concentration as a probe of mobility. Biophys. J. 16, 1315–1329.

Krishnan, R., Park, C.Y., Lin, Y.-.C., Mead, J., Jaspers, R.T., Trepat, X., Lenormand, G., Tambe, D., Smolensky, A.V., Knoll, A.H., 2009. Reinforcement versus fluidization in cytoskeletal mechanoresponsiveness. PLoS One 4, e5486.

Lakes, R., Vanderby, R., 1999. Interrelation of creep and relaxation: a modeling approach for ligaments. J. Biomech. Eng. 121, 612–615.

Lee, S.-.L., Nekouzadeh, A., Butler, B., Pryse, K.M., McConnaughey, W.B., Nathan, A.C., Legant, W.R., Schaefer, P.M., Pless, R.B., Elson, E.L., 2012. Physically-induced cytoskeleton remodeling of cells in three-dimensional culture. PLoS One 7, e45512.

Levental, K.R., Yu, H., Kass, L., Lakins, J.N., Egeblad, M., Erler, J.T., Fong, S.F.T., Csiszar, K., Giaccia, A., Weninger, W., 2009. Matrix crosslinking forces tumor progression by enhancing integrin signaling. Cell 139, 891–906.

Lin, Y., Hu, B., 2006. Load relaxation of a flat rigid circular indenter on a gel half space. J. Non Cryst. Solids 352, 4034–4040.

Lin, W.C., Shull, K.R., Hui, C.Y., Lin, Y.Y., 2007. Contact measurement of internal fluid flow within poly(n-isopropylacrylamide) gels. J. Chem. Phys. 127, 094906.

Magde, D., Elson, E.L., Webb, W.W., 1974. Fluorescence correlation spectroscopy. II. an experimental realization. Biopolym.: Orig. Res. Biomol. 13, 29–61.
Mak, A.F., Lai, W.M., Mow, V.C., 1987. Biphasic indentation of articular cartilage–I. Theoretical analysis. J. Biomech. 20, 703–714.
Malandrino, A., Jackson, A.R., Huyghe, J.M., Noailly, J., 2015. Poroelastic modeling of the intervertebral disc: a path toward integrated studies of tissue biophysics and organ degeneration. MRS Bull. 40, 324–332.
Malay, S., Rameshbabu, C.S., 2012. Collateral pathways in portal hypertension. J.Clin. Exp. Hepatol. 2, 338–352.
Marchesseau, S., Heimann, T., Chatelin, S., Willinger, R., Delingette, H., 2010. Fast porous visco-hyperelastic soft tissue model for surgery simulation: application to liver surgery. Prog. Biophys. Mol. Biol. 103, 185–196.
Mattice, J.M., Lau, A.G., Oyen, M.L., Kent, R.W., 2011. Spherical indentation load-relaxation of soft biological tissues. J. Mater. Res. 21, 2003–2010.
Mauck, R.L., Hung, C.T., Ateshian, G.A., 2003. Modeling of neutral solute transport in a dynamically loaded porous permeable gel: implications for articular cartilage biosynthesis and tissue engineering. J. Biomech. Eng. 125, 602–614.
Moeendarbary, E., Valon, L., Fritzsche, M., Harris, A.R., Moulding, D.A., Thrasher, A.J., Stride, E., Mahadevan, L., Charras, G.T., 2013. The cytoplasm of living cells behaves as a poroelastic material. Nat. Mater. 12, 253–261.
Mow, V.C., Hayes, W.C., 1991. Basic Orthopaedic Biomechanics. Raven Pr.
Mow, V.C., Holmes, M.H., Lai, W.M., 1984. Fluid transport and mechanical properties of articular cartilage: a review. J. Biomech. 17, 377–394.
Mow, V.C., Kuei, S.C., Lai, W.M., Armstrong, C.G., 1980a. Biphasic creep and stress relaxation of articular cartilage in compression: theory and experiments. J. Biomech. Eng. 102, 73.
Mow, V.C., Kuei, S.C., Lai, W.M., Armstrong, C.G., 1980b. Biphasic creep and stress relaxation of articular cartilage in compression? theory and experiments. J. Biomech. Eng. 102, 73–84.
Müller, A, Wapler, M C, Wallrabe, U, 2019. A quick and accurate method to determine the Poisson's ratio and the coefficient of thermal expansion of PDMS. Soft Matter 15, 779–784.
Nekouzadeh, A., Pryse, K.M., Elson, E.L., Genin, G.M., 2008. Stretch-activated force shedding, force recovery, and cytoskeletal remodeling in contractile fibroblasts. J. Biomech. 41, 2964–2971.
Nia, H.T., Han, L., Li, Y., Ortiz, C., Grodzinsky, A., 2011. Poroelasticity of cartilage at the nanoscale. Biophys. J. 101, 2304–2313.
Nicolle, S., Noguer, L., Palierne, J.F., 2012. Shear mechanical properties of the spleen: experiment and analytical modelling. J. Mech. Behav. Biomed. Mater. 9, 130–136.
Osterhoff, G., Morgan, E.F., Shefelbine, S.J., Karim, L., McNamara, L.M., Augat, P., 2016. Bone mechanical properties and changes with osteoporosis. Injury 47, S11–S20.
Oyen, M.L., 2011. Poroelastic nanoindentation responses of hydrated bone. J. Mater. Res. 23, 1307–1314.
Oyen, M.L., 2013. Nanoindentation of biological and biomimetic materials. Exp. Tech. 37, 73–87.
Oyen, M.L., 2015. Nanoindentation of hydrated materials and tissues. Curr. Opin. Solid State Mater. Sci. 19, 317–323.
Palmeri, M.L., Wang, M.H., Dahl, J.J., Frinkley, K.D., Nightingale, K.R., 2008. Quantifying hepatic shear modulus in vivo using acoustic radiation force. Ultrasound Med. Biol. 34, 546–558.
Provenzano, P., Lakes, R., Corr, D., Vanderby, R., 2002. Application of nonlinear viscoelastic models to describe ligament behavior. Biomech. Model. Mechanobiol. 1, 45–57.
Provenzano, P., Lakes, R., Keenan, T., 2001. Nonlinear ligament viscoelasticity. Ann. Biomed. Eng. 29, 908–914.
Ricken, T., Dahmen, U., Dirsch, O., 2010. A biphasic model for sinusoidal liver perfusion remodeling after outflow obstruction. Biomech. Model. Mechanobiol. 9, 435–450.
Rowe, R.A., Pryse, K.M., Elson, E.L., Genin, G.M., 2019. Stable fitting of noisy stress relaxation data. Mech. Soft Mater. 1, 9.
Rudnicki, J.W., 2001. Linear poroelasticity. In: Handbook of Materials Behavior Models. Academic Press, pp. 1118–1125.
Schuppan, D., Afdhal, N.H., 2008. Liver cirrhosis. Lancet 371, 838–851.
Simon, B.R., 1992. Multiphase poroelastic finite element models for soft tissue structures. Appl. Mech. Rev. 45, 191–218.
Sneddon, I.N., 1965. The relation between load and penetration in the axisymmetric boussinesq problem for a punch of arbitrary profile. Int. J. Eng. Sci. 3, 47–57.
Stock, R.J., Cilento, E.V., Mccuskey, R.S., 2010. A quantitative study of fluorescein isothiocyanate-dextran transport in the microcirculation of the isolated perfused rat liver. Hepatology 9, 75–82.
Strange, D.G.T., Fletcher, T.L., Tonsomboon, K., Brawn, H., Zhao, X., Oyen, M.L., 2013. Separating poroviscoelastic deformation mechanisms in hydrogels. Appl. Phys. Lett. 102, 031913.
Takigawa, T, Morino, Y, Urayama, K, et al., 1996. Poisson's ratio of polyacrylamide (PAAm) gels. Polym. Gels Networks 4, 1–5.
Umale, S., Deck, C., Bourdet, N., Dhumane, P., Soler, L., Marescaux, J., Willinger, R., 2013. Experimental mechanical characterization of abdominal organs: liver, kidney & spleen. J. Mech. Behav. Biomed. Mater. 17, 22–33.
Urayama, K., Takigawa, T., Masuda, T., 1993. Poisson's ratio of poly(vinyl alcohol) gels. Macromolecules 26, 3092–3096.
Wang, Q.-.M., Mohan, A.C., Oyen, M.L., Zhao, X.-.H., 2014. Separating viscoelasticity and poroelasticity of gels with different length and time scales. Acta Mech. Sin. 30, 20–27.
Wells, R.G., 2013. Tissue mechanics and fibrosis. Biochim. Biophys. Acta 1832, 884–890.
Xiang, H., Wang, P., Huang, G., Liu, S., Xu, M., Feng, X., Lu, T.J., 2013. Development of a micro-indentation device for measuring the mechanical properties of soft materials. Theor. Appl. Mech. Lett. 3, 054004.
Xu, B., Li, H., Zhang, Y., 2013. Understanding the viscoelastic behavior of collagen matrices through relaxation time distribution spectrum. Biomatter 3, e24651.
Yasuda, H., Lamaze, C. E., Peterlin, A., 1971. Diffusive and hydraulic permeabilities of water in water-swollen polymer membranes. J. Polym. Sci. Pol. Phys. 9, 1117–1131.
Youhua, L., 2006. Renal fibrosis: new insights into the pathogenesis and therapeutics. Kidney Int. 69, 213–217.